

Histogram of Gradient Orientations of Signal Plots applied to P300 Detection

Rodrigo Ramele^{1,*}, Ana Julia Villar¹ and Juan Miguel Santos¹

¹*Centro de Inteligencia Computacional, Computer Engineering Department, Instituto Tecnológico de Buenos Aires (ITBA), Buenos Aires, Argentina*

Correspondence*:

Rodrigo Ramele, C1437FBH Lavarden 315, Ciudad Autónoma de Buenos Aires, Argentina
rramele@itba.edu.ar

2 ABSTRACT

3 Word Count: 6144

4 The analysis of Electroencephalographic (EEG) signals is of ulterior importance to aid in the
5 diagnosis of mental disease and to increase our understanding of the brain. Traditionally, clinical
6 EEG has been analyzed in terms of temporal waveforms, looking at rhythms in spontaneous
7 activity, subjectively identifying troughs and peaks in Event-Related Potentials (ERP), or by
8 studying graphoelements in pathological sleep stages. Additionally, the discipline of Brain
9 Computer Interfaces (BCI) requires new methods to decode patterns from non-invasive EEG
10 signals. This field is developing alternative communication pathways to transmit volitional
11 information from the Central Nervous System. The technology could potentially enhance the
12 quality of life of patients affected by neurodegenerative disorders and other mental illness. This
13 work mimics what electroencephalographers have been doing clinically, visually inspecting and
14 categorizing phenomena within the EEG by the extraction of features from images of signal plots.
15 These features are constructed based on the calculation of histograms of oriented gradients
16 from pixels around the signal plot. It aims to provide a new objective framework to analyze,
17 characterize and classify EEG signal waveforms. The feasibility of the method is outlined by
18 detecting the P300, an ERP elicited by the oddball paradigm of rare events, and implementing
19 an offline P300-based BCI Speller. The validity of the proposal is shown by offline processing a
20 public dataset of Amyotrophic Lateral Sclerosis (ALS) patients and an own dataset of healthy
21 subjects.

22 **Keywords:** electroencephalography, histogram of gradient orientations, brain-computer interfaces, P300, SIFT, amyotrophic lateral
23 sclerosis, naive-bayes near neighbours, waveforms

1 INTRODUCTION

24 Although recent advances in neuroimaging techniques, particularly radio-nuclear and radiological
25 scanning methods (Schomer and Silva, 2010), have diminished the prospects of the traditional
26 Electroencephalography, the advent and development of digitized devices has impelled for a revamping of
27 this hundred years old technology. Their versatility, ease of use, temporal resolution, ease of development
28 and production, and its proliferation as consumer devices, are pushing EEG to become the de-facto non

29 invasive portable or ambulatory method to access and harness brain information (De Vos and Debener,
30 2014).

31 A key contribution to this expansion has been the field of Brain Computer Interfaces (Wolpaw and E.,
32 2012) which is the pursuit of the development of a new channel of communication particularly aimed to
33 persons affected by neurodegenerative diseases.

34 One noteworthy aspect of this novel communication channel is the ability to transmit information from
35 the Central Nervous System (CNS) to a computer device and from there use that information to control a
36 wheelchair (Carlson and del R. Millan, 2013), as input to a speller application (Guger et al., 2009), in a
37 Virtual Reality environment (Lotte et al., 2013) or as aiding tool in a rehabilitation procedure (Jure et al.,
38 2016). The holly grail of BCI is to implement a new complete and alternative pathway to restore lost
39 locomotion (Wolpaw and E., 2012).

40 EEG signals are remarkably complex and have been characterized as a multichannel non-stationary
41 stochastic process. Additionally, they have high variability between different subjects and even between
42 different moments for the same subject, requiring adaptive and co-adaptive calibration and learning
43 procedures (Clerc et al., 2016). Hence, this imposes an outstanding challenge that is necessary to overcome
44 in order to extract information from raw EEG signals.

45 BCI has gained mainstream public awareness with worldwide challenge competitions like
46 Cybathlon (Riener and Seward, 2014; Novak et al., 2018) and even been broadcasted during the inauguration
47 ceremony of the 2014 Soccer World Cup. New developments have overcome the out-of-the-lab high-bar
48 and they are starting to be used in real world environments (Guger et al., 2017; Huggins et al., 2016).
49 However, they still lack the necessary robustness, and its performance is well behind any other method of
50 human computer interaction, including any kind of detection of residual muscular movement (Clerc et al.,
51 2016).

52 A few works have explored the idea of exploiting the signal waveform to analyze the EEG signal.
53 In (Alvarado-González et al., 2016) an approach based on Slope Horizontal Chain Code is presented,
54 whereas in (Yamaguchi et al., 2009) a similar procedure was implemented based on Mathematical
55 Morphological Analysis. The seminal work of Bandt-Pompe Permutation Entropy (Berger et al., 2017) also
56 explores succinctly this idea as a basis to establish the time series ordinal patterns. In the article (Ramele
57 et al., 2016), the authors introduce a method for classification of rhythmic EEG events like Visual Occipital
58 Alpha Waves and Motor Imagery Rolandic Central μ Rhythms using the Histogram of Gradient Orientations
59 of signal plots. Inspired in that work, we propose a novel application of the developed method to classify
60 and describe transient events, particularly the P300 Event Related Potential. The proposed approach is
61 based on the waveform analysis of the shape of the EEG signal. The signal is drawn on a bidimensional
62 image plot, vector gradients of pixels around the plot are obtained, and with them, the histogram of their
63 orientations is calculated. This histogram is a direct representation of the waveform of the signal. The
64 method is built by mimicking what regularly electroencephalographers have been performing for almost a
65 century as it is described in (Hartman, 2005): visually inspecting raw signal plots.

66 This paper reports a method to, (1) describe a procedure to capture the shape of a waveform of an ERP
67 component, the P300, using histograms of gradient orientations extracted from images of signal plots,
68 and (2) outline the way in which this procedure can be used to implement an P300-Based BCI Speller
69 application. Its validity is verified by offline processing two datasets, one of data from ALS patients and
70 another one from data of healthy subjects.

This article unfolds as follows: Section 2.1 is dedicated to explain the Feature Extraction method based on Histogram of Gradient Orientations of the Signal Plot: Section 2.1.1 shows the preprocessing pipeline, Section 2.1.2 describes the image generation of the signal plot, Section 2.1.3 presents the feature extraction procedure while Section 2.1.4 introduces the Speller Matrix Letter Identification procedure. In Section 2.2, the experimental protocol is expounded. Section 3 shows the results of applying the proposed technique. In the final Section 4 we expose our remarks, conclusions and future work.

2 MATERIALS AND METHODS

The P300 (Farwell and Donchin, 1988; Knuth et al., 2006) is a positive deflection of the EEG signal which occurs around 300 ms after the onset of a rare and deviant stimulus that the subject is expected to attend. It is produced under the oddball paradigm (Wolpaw and E., 2012) and it is consistent across different subjects. It has a lower amplitude ($\pm 5\mu V$) compared to basal EEG activity, reaching a Signal to Noise Ratio (SNR) of around -15 db estimated based on the amplitude of the P300 response signal divided by the standard deviation of the background EEG activity (Hu et al., 2010). This signal can be used to implement a speller application by means of a Speller Matrix (Farwell and Donchin, 1988). This matrix is composed of 6 rows and 6 columns of numbers and letters. The subject can focus on one character of the matrix. Figure 1 shows an example of the Speller Matrix used in the OpenVibe open source software (Renard et al., 2010), where the flashes of rows and columns provide the deviant stimulus required to elicit this physiological response. Each time a row or a column that contains the desired letter flashes, the corresponding synchronized EEG signal should also contain the P300 signature and by detecting it, the selected letter can be identified.

2.1 Feature Extraction from Signal Plots

In this section, the signal preprocessing, the method for generating images from signal plots, the feature extraction procedure and the Speller Matrix identification are described. Figure 2 shows a scheme of the entire process.

2.1.1 Preprocessing Pipeline

The data obtained by the capturing device is digitalized and a multichannel EEG signal is constructed. The 6 rows and 6 columns of the Speller Matrix are intensified providing the visual stimulus. The number of a row or column is a location. A sequence of twelve randomly permuted locations l conform an intensification sequence. The whole set of twelve intensifications is repeated k_a times.

• **Signal Enhancement:** This stage consists of the enhancement of the SNR of the P300 pattern above the level of basal EEG. The pipeline starts by applying a notch filter to the raw digital signal, a 4th degree 10 Hz lowpass Butterworth filter and finally a decimation with a Finite Impulse Response (FIR) filter of order 30 from the original sampling frequency down to 16 Hz (Krusienski et al., 2006).

• **Artifact Removal:** For every complete sequence of 12 intensifications of 6 rows and 6 columns, a basic artifact elimination procedure is implemented by removing the entire sequence when any signal deviates above/below $\pm 70\mu V$.

• **Segmentation:** For each of the 12 intensifications of one intensification sequence, a segment S_i^l of a window of t_{max} seconds of the multichannel signal is extracted, starting from the stimulus onset, corresponding to each row/column intensification l and to the intensification sequence i . As intensifications are permuted in a random order, the segments are rearranged corresponding to row flickering, labeled 1-6, whereas those corresponding to column flickering are labeled 7-12. Two of

110 these segments should contain the P300 ERP signature time-locked to the flashing stimulus, one for
 111 the row, and one for the column.

- 112 • **Signal Averaging:** The P300 ERP is deeply buried under basal EEG so the standard approach to
 113 identify it is by point-to-point averaging the time-locked stacked signal segments. Hence the values
 114 which are not related to, and not time-locked to the onset of the stimulus are canceled out (Liang and
 115 Bougrain, 2008).

116 This last step determines the operation of any P300 Speller. In order to obtain an improved signal
 117 in terms of its SNR, repetitions of the sequence of row/column intensification are necessary. And,
 118 at the same time, as long as more repetitions are needed, the ability to transfer information faster is
 119 diminished, so there is a trade-off that must be acutely determined.

120 The procedure to obtain the point-to-point averaged signal goes as follows:

- 121 1. Highlight randomly the rows and columns from the matrix. There is one row and one column that
 122 should match the letter selected by the subject.
- 123 2. Repeat step 1 k_a times, obtaining the $1 \leq l \leq 12$ segments $S_1^l(n, c), \dots, S_{k_a}^l(n, c)$, of the EEG
 124 signal where the variables $1 \leq n \leq n_{max}$ and $1 \leq c \leq C$ correspond to sample points and channel,
 125 respectively. The parameter C is the number of available EEG channels whereas $n_{max} = F_s t_{max}$
 126 is the segment length and F_s is the sampling frequency. The parameter k_a is the number of
 127 repetitions of intensifications and it is an input parameter of the algorithm.
- 128 3. Compute the Ensemble Average by

$$x^l(n, c) = \frac{1}{k_a} \sum_{i=1}^{k_a} S_i^l(n, c) \quad (1)$$

129 for $1 \leq n \leq n_{max}$ and for the channels $1 \leq c \leq C$. This provide an averaged signal $x^l(n, c)$ for
 130 the twelve locations $1 \leq l \leq 12$.

131 2.1.2 Signal Plotting

132 Averaged signal segments are standardized and scaled for $1 \leq n \leq n_{max}$ and $1 \leq c \leq C$ by

$$\tilde{x}^l(n, c) = \left[\gamma \frac{(x^l(n, c) - \bar{x}^l(c))}{\hat{\sigma}^l(c)} \right] \quad (2)$$

where $\gamma > 0$ is an input parameter of the algorithm and it is related to the image scale. In addition, $x^l(n, c)$ is the point-to-point averaged multichannel EEG signal for the sample point n and for channel c . Lastly,

$$\bar{x}^l(c) = \frac{1}{n_{max}} \sum_{n=1}^{n_{max}} x^l(n, c)$$

and

$$\hat{\sigma}^l(c) = \left\{ \frac{1}{n_{max} - 1} \sum_{n=1}^{n_{max}} [x^l(n, c) - \bar{x}^l(c)]^2 \right\}^{\frac{1}{2}}$$

133 are the mean and estimated standard deviation of $x^l(n, c)$, $1 \leq n \leq n_{max}$, for each channel c .

134 Consequently, a binary image $I^{(l,c)}$ is constructed according to

$$I^{(l,c)}(z_1, z_2) = \begin{cases} 255 & \text{if } z_1 = \gamma n \quad \text{and} \quad z_2 = \tilde{x}^l(n, c) + z^l(c) \\ 0 & \text{otherwise} \end{cases} \quad (3)$$

135 with 255 being white and representing the signal's value location and 0 for black which is the background
 136 contrast, conforming a black-and-white plot of the signal. Pixel arguments $(z_1, z_2) \in \mathbb{N} \times \mathbb{N}$ iterate over
 137 the width (based on the length of the signal segment) and height (based on the peak-to-peak amplitude) of
 138 the newly created image with $1 \leq n \leq n_{max}$ and $1 \leq c \leq C$. The value $z^l(c)$ is the image vertical position
 139 where the signal's zero value has to be situated in order to fit the entire signal within the image for each
 140 channel c:

$$z^l(c) = \left\lfloor \frac{\max_n \tilde{x}^l(n, c) - \min_n \tilde{x}^l(n, c)}{2} \right\rfloor - \left\lfloor \frac{\max_n \tilde{x}^l(n, c) + \min_n \tilde{x}^l(n, c)}{2} \right\rfloor \quad (4)$$

141 where the minimization and maximization are carried out for n varying between $1 \leq n \leq n_{max}$, and $\lfloor \cdot \rfloor$
 142 denote the rounding to the smaller nearest integer of the number.

143 In order to complete the plot $I^{(l,c)}$ from the pixels, the Bresenham (Bresenham, 1965; Ramele et al.,
 144 2016) algorithm is used to interpolate straight lines between each pair of consecutive pixels.

145 2.1.3 Feature Extraction: Histogram of Gradient Orientations

146 The work of Edelman, Intrator and Poggio (Hubel and Wiesel, 1962) on how the visual cortex sense
 147 features was the inspiration to the development of an algorithm to identify and decode salient local
 148 information from image regions. The Scale Invariant Feature Transform (SIFT) is a Computer Vision
 149 method proposed by Lowe (2004) which is composed of two parts, the SIFT Detector and the SIFT
 150 Descriptor. The former is the procedure to identify relevant areas of an image whereas the latter is the
 151 procedure to describe and characterize a region of an image (i.e. patch) calculating an histogram of the
 152 angular orientations of pixel gradients. In order to characterize EEG signal waveforms, this work proposes
 153 an alternative to the SIFT Descriptor, the Histogram of Gradient Orientations(HIST) algorithm.

154 For each generated image $I^{(l,c)}$, a keypoint p_k is placed on a pixel (x_{p_k}, y_{p_k}) over the image plot and a
 155 window around the keypoint is considered: a local image patch. Its size is $X_p \times X_p$ pixels and is constructed
 156 by dividing the window in 16 blocks of size $3s$ each one, where s is the scale of the local patch and it is an
 157 input parameter of the algorithm. It is arranged in a 4×4 grid and the pixel p_k is the patch center, thus
 158 $X_p = 12s$ pixels.

159 A local representation of the signal shape within the patch can be described by obtaining the gradient
 160 orientations on each of the 16 blocks $B_{i,j}$ with $0 \leq i, j \leq 3$ and creating a histogram of gradients. In
 161 order to calculate the histogram, the interval $[0, 360]$ of possible angles is divided in 8 bins, each one of 45
 162 degrees.

163 Hence, for each spatial bin $0 \leq i, j \leq 3$, corresponding to the indexes of each block $B_{i,j}$, the orientations
 164 are accumulated in a 3-dimensional histogram h through the following equation:

$$h(\theta, i, j) = 3s \sum_{\mathbf{p} \in I^{(l,c)}} w_{ang}(\angle J(\mathbf{p}) - \theta) w_{ij} \left(\frac{\mathbf{p} - \mathbf{p}_k}{3s} \right) \|J(\mathbf{p})\| \quad (5)$$

165 where \mathbf{p} is a pixel from the image $I^{(l,c)}$, θ is the angle bin with $\theta \in \{0, 45, 90, 135, 180, 225, 270, 315\}$,
 166 $\|J(\mathbf{p})\|$ is the euclidean norm of the gradient vector in the pixel \mathbf{p} and it is computed using finite differences
 167 and $\angle J(\mathbf{p})$ is the angle of the gradient vector.

168 The contribution of each gradient vector to the histogram calculated by Equation 5 is balanced by a
 169 trilinear interpolation. The scalar $w_{ang}(\cdot)$ and vector $w_{ij}(\cdot)$ functions are linear interpolations used by Lowe
 170 (2004) and Vedaldi and Fulkerson (2010) to provide a weighting contribution to the eight adjacent bins in
 171 the tridimensional histogram. They are calculated as

$$w_{ij}(\mathbf{v}) = w(v_x - x_i)w(v_y - y_j) \quad (6)$$

172 with $0 \leq i, j \leq 3$ and

$$w_{ang}(\alpha) = \sum_{r=-1}^1 w\left(\frac{8\alpha}{2\pi} + 8r\right) \quad (7)$$

173 where x_i and y_i are the spatial bin centers located in $x_i, y_i \in \{-\frac{3}{2}, -\frac{1}{2}, \frac{1}{2}, \frac{3}{2}\}$ and the interpolating function
 174 $w(\cdot)$ is defined as $w(z) = \max(0, 1 - |z|)$. The function parameter $\mathbf{v} = (v_x, v_y)$ is a vector variable and α
 175 a scalar variable. Vector \mathbf{v} holds pixel coordinates (v_x, v_y) normalized between -2 and 2 and combined
 176 with the function $w(z)$ it produces zero for every combination of (i, j) except for the 4 adjacent spatial
 177 bins. On the other hand, r is an integer that can vary freely in the set $\{-1, 0, 1\}$ and α is the difference
 178 between the gradient orientation angle and the angle bin center in radians. By following this procedure,
 179 summands on Equation 7 are nullified except for the 2 adjacent angular bins.

180 These binning functions conform the trilinear interpolation that has a combined effect of sharing the
 181 contribution of each oriented gradient between their eight adjacent bins in a tridimensional cube in the
 182 histogram space, and zero everywhere else (Mortensen et al., 2005).

183 The fixed value of 3 is a magnification factor which corresponds to the number of pixels per each
 184 block when $s = 1$. As the patch has 16 blocks and 8 bin angles are considered, for each location l and
 185 channel c a feature called *descriptor* $\mathbf{d}^{(l,c)}$ of 128 dimension is obtained. The main differences between
 186 this implementation and the standard SIFT Descriptor are described in the Appendix on Section 5.

187 Figure 3 shows an example of a patch and a scheme of the histogram computation. In (A) a plot of the
 188 signal and the patch centered around the keypoint is shown. In (B) the possible orientations on each patch
 189 are illustrated. Only the upper-left four blocks are visible. The first eight orientations of the first block, are
 190 labeled from 1 to 8 clockwise. The orientations of the second block $B_{1,2}$ are labeled from 9 to 16. This
 191 labeling continues left-to-right, up-down until the eight orientations for all the sixteen blocks are assigned.
 192 They form the corresponding descriptor \mathbf{d} of 128 coordinates. Finally, in (C) an enlarged image plot is
 193 shown where the oriented gradient vector for each pixel can be seen.

194 2.1.4 Speller Matrix letter Identification

195 2.1.4.1 P300 ERP Extraction

196 Segments corresponding to row flickering are labeled 1-6, whereas those corresponding to column
 197 flickering are labeled 7-12. The extraction process has the following steps:

- **Step A:** First highlight rows and columns from the matrix in a random permutation order and obtain the Ensemble Average as detailed in steps 1, 2 and 3 in Section 2.1.1.
- **Step B:** Plot the signals $\tilde{x}^l(n, c)$, $1 \leq n \leq n_{max}$, $1 \leq c \leq C$, according Section 2.1.2 in order to generate the images $I^{(l,c)}$ for rows and columns $1 \leq l \leq 12$.
- **Step C:** Obtain the descriptors $\mathbf{d}^{(l,c)}$ for rows and columns from $I^{(l,c)}$ in accordance to the method described in Section 2.1.3.

2.1.4.2 Calibration

A trial, as defined by the BCI2000 platform (Schalk et al., 2004), is every attempt to select just one letter from the speller. A set of trials is used for calibration and once the calibration is complete it can be used to identify new letters from new trials.

During the calibration phase, two descriptors $\mathbf{d}^{(l,c)}$ are extracted for each available channel, corresponding to the locations l of a selection of one previously instructed letter from the set of calibration trials. These descriptors are the P300 templates, grouped together in a template set called T^c . The set is constructed using the steps described in Section 2.1.1 and the steps A, B and C of the P300 ERP extraction process.

Additionally, the best performing channel, bpc is identified based on the the channel where the best Character Recognition Rate is obtained.

2.1.4.3 Letter identification

In order to identify the selected letter, the template set T^{bpc} is used as a database. Thus, new unclassified descriptors $\mathbf{q}^{(l,bpc)}$ are computed and they are compared against the descriptors belonging to the calibration template set T^{bpc} .

The Naive Bayes Nearest Neighbor (k-NBNN) (Boiman et al., 2008) is a discriminative (Wolpaw and E., 2012) semi-supervised classification algorithm that allows the categorization of an image to one class by comparing the set of extracted descriptors to those which are more similar from template dictionaries. This work proposes an adapted version to obtain a unary classification scheme to identify the selected letter in the P300-Based BCI Speller, based on the features provided by the calculated descriptors.

- **Step D:** Match to the calibration template T^{bpc} by computing

$$\hat{row} = \arg \min_{l \in \{1, \dots, 6\}} \sum_{h=1}^k \left\| \mathbf{q}^{(l,bpc)} - \mathbf{d}_h^{(bpc)} \right\|^2 \quad (8)$$

and

$$\hat{col} = \arg \min_{l \in \{7, \dots, 12\}} \sum_{h=1}^k \left\| \mathbf{q}^{(l,bpc)} - \mathbf{d}_h^{(bpc)} \right\|^2 \quad (9)$$

with $\mathbf{d}_h^{(bpc)}$ belonging to the set $N_T(\mathbf{q}^{(l,bpc)})$, which is defined, for the best performing channel, as $N_T(\mathbf{q}^{(l,bpc)}) = \{\mathbf{d}_h^{(bpc)} \in T^{bpc} / \mathbf{d}_h^{(bpc)} \text{ is the } k\text{-nearest neighbor of } \mathbf{q}^{(l,bpc)}\}$. This set is obtained by sorting all the elements in T^{bpc} based on distances between them and $\mathbf{q}^{(l,bpc)}$, choosing the k with smaller values, with k a parameter of the algorithm.

By computing the aforementioned equations, the letter of the matrix can be determined from the intersection of the row \hat{row} and column \hat{col} . Figure 2 shows a scheme of this process.

231 2.2 Experimental Protocol

232 To verify the validity of the proposed framework and method, the public dataset 008-2014 (Riccio et al.,
233 2013) published on the BNCI-Horizon website (Brunner et al., 2014) by IRCCS Fondazione Santa Lucia,
234 is used. Additionally, an own dataset with the same experimental conditions is generated. Both of them are
235 utilized to perform an offline BCI Simulation to decode the spelled words from the provided signals.

236 The algorithm is implemented on MATLAB V2017a (Mathworks Inc., Natick, MA, USA). The algorithm
237 described in 2.1.3 is implemented on a modified version of the VLFeat (Vedaldi and Fulkerson, 2010)
238 Computer Vision library. Furthermore, in order to enhance the impact of this paper and for a sake of
239 reproducibility, the code of the entire algorithm, including the modified VLFeat library, has been made
240 available at: <https://bitbucket.org/itba/hist>.

241 In the following sections the characteristics of the datasets and parameters of the identification algorithm
242 are described.

243 2.2.1 P300 ALS Public Dataset

244 The experimental protocol used to generate this dataset is explained in (Riccio et al., 2013) but can
245 be summarized as follows: 8 subjects with confirmed diagnoses but on different stages of ALS disease,
246 were recruited and accepted to perform the experiments. The Visual P300 detection task designed for this
247 experiment consisted of spelling 7 words of 5 letters each, using the traditional P300 Speller Matrix (Farwell
248 and Donchin, 1988). The flashing of rows and columns provide the deviant stimulus required to elicit this
249 physiological response. The first 3 words are used for calibration and the remaining 4 words, for testing
250 with visual feedback. A trial is every attempt to select a letter from the speller. It is composed of signal
251 segments corresponding to $k_a = 10$ repetitions of flashes of 6 rows and $k_a = 10$ repetitions of flashes of 6
252 columns of the matrix, yielding 120 repetitions. Flashing of a row or a column is performed for 0.125s,
253 following by a resting period (i.e. inter-stimulus interval) of the same length. After 120 repetitions an
254 inter-trial pause is included before resuming with the following letter.

255 The recorded dataset was sampled at 256 Hz and it consisted of a scalp multichannel EEG signal for
256 electrode channels Fz, Cz, Pz, Oz, P3, P4, PO7 and PO8, identified according to the 10-20 International
257 System, for each one of the 8 subjects. The recording device was a research-oriented digital EEG device
258 (g.Mobilab, g.Tec, Austria) and the data acquisition and stimuli delivery were handled by the BCI2000
259 open source software (Schalk et al., 2004).

260 In order to assess and verify the identification of the P300 response, subjects are instructed to perform a
261 copy-spelling task. They have to fix their attention to successive letters for copying a previously determined
262 set of words, in contrast to a free-running operation of the speller where each user decides on its own what
263 letter to choose.

264 2.2.2 P300 for healthy subjects

265 We replicate the same experiment on healthy subjects using a wireless digital EEG device (g.Nautilus,
266 g.Tec, Austria). The experimental conditions are the same as those used for the previous dataset, as detailed
267 in section 2.2.1. The produced dataset is available in a public online repository (Ramele et al., 2017).

268 Participants are recruited voluntarily and the experiment is conducted anonymously in accordance with
269 the Declaration of Helsinki published by the World Health Organization. No monetary compensation
270 is handed out and all participants agree and sign a written informed consent. This study is approved
271 by the *Departamento de Investigación y Doctorado, Instituto Tecnológico de Buenos Aires (ITBA)*. All

272 healthy subjects have normal or corrected-to-normal vision and no history of neurological disorders. The
 273 experiment is performed with 8 subjects, 6 males, 2 females, 6 right-handed, 2 left-handed, average age
 274 29.00 years, standard deviation 11.56 years, range 20-56 years.

275 EEG data is collected in a single recording session. Participants are seated in a comfortable chair, with
 276 their vision aligned to a computer screen located one meter in front of them. The handling and processing
 277 of the data and stimuli is conducted by the OpenVibe platform (Renard et al., 2010).

278 Gel-based active electrodes (g.LADYbird, g.Tec, Austria) are used on the same positions Fz, Cz, Pz,
 279 Oz, P3,P4, PO7 and PO8. Reference is set to the right ear lobe and ground is preset as the AFz position.
 280 Sampling frequency is slightly different, and is set to 250 Hz, which is the closest possible to the one used
 281 with the other dataset.

282 2.2.3 Parameters

283 The patch size is $X_P = 12s \times 12s$ pixels, where s is the scale of the local patch and it is an input parameter
 284 of the algorithm. The P300 event can have a span of 400 ms and its amplitude can reach $10\mu V$ (Rao, 2013).
 285 Hence it is necessary to utilize a signal segment of size $t_{max} = 1$ second and a size patch X_P that could
 286 capture an entire transient event. With this purpose in consideration, the s value election is essential.

287 We propose the Equations 10 and 11 to compute the scale value in horizontal and vertical directions,
 288 respectively.

$$s_x = \frac{\gamma \lambda F_s}{12} \quad (10)$$

$$s_y = \frac{\gamma \Delta\mu V}{12} \quad (11)$$

289 where λ is the length in seconds covered by the patch, F_s is the sampling frequency of the EEG signal
 290 (downsampled to 16 Hz) and $\Delta\mu V$ corresponds to the amplitude in microvolts that can be covered by the
 291 height of the patch. The geometric structure of the patch is determined by the waveform to be captured,
 292 thus we discerned that by using $s = s_x = s_y = 3$ and $\gamma = 4$, the local patch and the descriptor can identify
 293 events of $9\mu V$ of amplitude, with a span of $\lambda = 0.56$ seconds. This also determines that 1 pixel represents
 294 $\frac{1}{\gamma} = \frac{1}{4}\mu V$ on the vertical direction and $\frac{1}{F_s \gamma} = \frac{1}{64}$ seconds on the horizontal direction. The keypoints p_k
 295 are located at $(x_{p_k}, y_{p_k}) = (0.55F_s \gamma, z^l(c)) = (35, z^l(c))$ for the corresponding channel c and location l
 296 (see Equation 4). In this way the whole transient event is captured. Figure 4 shows a patch of a signal plot
 297 covering the complete amplitude (vertical direction) and the complete span of the signal event (horizontal
 298 direction).

299 The number of channels C is equal to 8 for both datasets, and the number of intensification sequences k_a
 300 is fixed to 10. The parameter k used to construct the set $N_T(\mathbf{q}^{(l,c)})$ is assigned to $k = 7$, which was found
 301 empirically to achieve better results. In addition, the norm used on Equations 8 and 9 is the cosine norm,
 302 and descriptors are normalized to $[-1, 1]$.

303 Lastly, in order to assess the validity of the HIST method, the character recognition rate for both
 304 datasets is evaluated replicating the methodology proposed by the ALS dataset's publisher, since authors
 305 Riccio et al. (2013) did not report the Character Recognition Rate obtained for this dataset. Frequency
 306 filtering, data segmentation and artifact rejection is conducted according to Section 2.1.1 yielding 16 x
 307 8 samples per epoch. A multichannel feature consists of time points vector (Lotte et al., 2018), formed
 308 by concatenating all the channels (Krusienski et al., 2006). A single-channel variant consists of using

309 time points from a single electrode and performing the analysis on a channel-by-channel basis. Three
310 classification schemes are considered as well. A multichannel version of the Stepwise Linear Discriminant
311 Analysis (SWLDA) classification algorithm. SWLDA is the methodology proposed by the ALS dataset's
312 publisher. Additionally, a single-channel and a multichannel variant of a linear kernel Support Vector
313 Machine (SVM) (Scholkopf and Smola, 2001) classifier are utilized. SVM has been successfully used in
314 several BCI Competitions (Rakotomamonjy and Guigue, 2008).

3 RESULTS

315 Table 1 shows the results of applying the HIST algorithm to the subjects of the public dataset of ALS
316 patients. The percentage of correctly spelled letters is calculated while performing an offline BCI Simulation.
317 From the seven words for each subject, the first three are used for calibration, and the remaining four are
318 used for testing. The best performing channel *bpc* is informed as well. The target ratio is 1 : 36; hence
319 theoretical chance level is 2.8%. It can be observed that the best performance of the letter identification
320 method is reached in a dissimilar channel depending on the subject being studied. Table 1 and 2 show for
321 comparison the obtained performance rates using single-channel signals with the SVM classifier. The best
322 performing channel, where the best letter identification rate was achieved, is also depicted.

323 The Information Transfer Rate (ITR), or Bit Transfer Rate (BTR), in the case of reactive BCIs (Wolpaw
324 and E., 2012) depends on the amount of signal averaging required to transmit a valid and robust selection.
325 Figure 5 shows the performance curves for varying intensification sequences for the subjects included in
326 the dataset of ALS patients. It can be noticed that the percentage of correctly identified letters depends
327 on the number of intensification sequences that are used to obtain the averaged signal. Moreover, when
328 the number of intensification sequences tend to 1, which corresponds to single-intensification character
329 recognition, the performance is reduced. As mentioned before, the SNR of the P300 obtained from only
330 one segment of the intensification sequence is very low and the shape of its P300 component is not very
331 well defined.

332 In Table 2 the results obtained for 8 healthy subjects are shown. It can be observed that the performance
333 is above chance level. It is verified that HIST method has an improved performance at letter identification
334 than SVM that process the signals on a channel by channel strategy (Wilcoxon signed-rank test, $p = 0.004$
335 for both datasets).

336 Tables 3 and 4 are presented in order to compare the performance of the HIST method versus multichannel
337 SWLDA and SVM classification algorithms for both datasets. It is verified for the dataset of ALS patients
338 that it has similar performance against other methods like SWLDA or SVM, which use a multichannel
339 feature (Quade test with $p = 0.55$) whereas for the dataset of healthy subjects significant differences are
340 found (Quade test with $p = 0.02$) where only the HIST method achieves a different performance than SVM
341 (with multiple comparisons, significant difference of level 0.05).

342 The P300 ERP consists of two overlapping components: the P3a and P3b, the former with frontocentral
343 distribution while the later stronger on centroparietal region (Polich, 2007). Hence, the standard practice is
344 to find the stronger response on the central channel Cz (Riccio et al., 2013). However, Krusienski et al.
345 (2006) show that the response may also arise in occipital regions. We found that by analyzing only the
346 waveforms, occipital channels PO8 and PO7 show higher performances for some subjects.

347 As subjects have varying *latencies* and *amplitudes* of their P300 components, they also have a varying
348 stability of the *shape* of the generated ERP (Nam et al., 2010). Figure 6 shows 10 sample P300 templates
349 patches for patients 8 and 3 from the dataset of ALS patients. It can be discerned that in coincidence with

350 the performance results, the P300 signature is more clear and consistent for subject 8 (A) while for subject
351 3 (B) the characteristic pattern is more difficult to perceive.

352 Additionally, the stability of the P300 component waveform has been extensively studied in patients
353 with ALS (Sellers et al., 2006; Madarame et al., 2008; Nijboer and Broermann, 2009; Mak et al., 2012;
354 McCane et al., 2015) where it was found that these patients have a stable P300 component, which were
355 also sustained across different sessions. In line with these results we do not find evidence of a difference in
356 terms of the performance obtained by analyzing the waveforms (HIST) for the group of patients with ALS
357 and the healthy group of volunteers (Mann-Whitney U Test, $p = 0.46$). Particularly, the best performance
358 is obtained for a subject from the ALS dataset for which, based on visual observation, the shape of they
359 P300 component is consistently identified.

360 It is important to remark that when applied to binary images obtained from signal plots, the feature
361 extraction method described in Section 2.1.3 generates sparse descriptors. Under this subspace we found
362 that using the cosine metric yielded a significant performance improvement. On the other hand, the unary
363 classification scheme based on the NBNN algorithm proved very beneficial for the P300 Speller Matrix.
364 This is due to the fact that this approach solves the unbalance dataset problem which is inherent to the
365 oddball paradigm (Tibon and Levy, 2015).

4 DISCUSSION

366 Among other applications of Brain Computer Interfaces, the goal of the discipline is to provide
367 communication assistance to people affected by neuro-degenerative diseases, who are the most likely
368 population to benefit from BCI systems and EEG processing and analysis.

369 In this work, a method to extract an objective metric from the waveform of the plots of EEG signals is
370 presented. Its usage to implement a valid P300-Based BCI Speller application is expounded. Additionally,
371 its validity is evaluated using a public dataset of ALS patients and an own dataset of healthy subjects.

372 It was verified that this method has an improved performance at letter identification than other methods
373 that process the signals on a channel by channel strategy, and it even has a comparable performance against
374 other methods like SWLDA or SVM, which uses a multichannel feature. Furthermore, this method has the
375 advantage that shapes of waveforms can be analyzed in an objective way. We observed that the shape of
376 the P300 component is more stable in occipital channels, where the performance for identifying letters
377 is higher. We additionally verified that ALS P300 signatures are stable in comparison to those of healthy
378 subjects.

379 We believe that the use of descriptors based on histogram of gradient orientation, presented in this work,
380 can also be utilized for deriving a shape metric in the space of the P300 signals which can complement
381 other metrics based on time-domain as those defined by Mak et al. (2012). It is important to notice
382 that the analysis of waveform shapes is usually performed in a qualitative approach based on visual
383 inspection (Sellers et al., 2006), and a complementary methodology which offer a quantitative metric will
384 be beneficial to these routinely analysis of the waveform of ERPs.

385 The goal of this work is to answer the question if a P300 component could be solely determined by
386 inspecting automatically their waveforms. We conclude affirmatively, though two very important issues
387 still remain:

388 First, the stability of the P300 in terms of its shape is crucial: the averaging procedure, montages, the
389 signal to noise ratio and spatial filters all of them are non-physiological factors that affect the stability of

390 the shape of the P300 ERP. We tested a preliminary approach to assess if the morphological shape of the
391 P300 of the averaged signal can be stabilized by applying different alignments of the stacked segments (see
392 Figure 2) and we verified that there is a better performance when a correct segment alignment is applied.
393 We applied Dynamic Time Warping (DTW) (Casarotto et al., 2005) to automate the alignment procedure
394 but we were unable to find a substantial improvement. Further work to study the stability of the shape of
395 the P300 signature component needs to be addressed.

396 The second problem is the amplitude variation of the P300. We propose a solution by standardizing the
397 signal, shown in Equation 2. It has the effect of normalizing the peak-to-peak amplitude, moderating its
398 variation. It has also the advantage of reducing noise that was not reduced by the averaging procedure. It is
399 important to remark that the averaged signal variance depends on the number of segments used to compute
400 it (Van Drongelen, 2006). The standardizing process converts the signal to unit signal variance which
401 makes it independent of the number k_a of signals averaged. Although this is initially an advantageous
402 approach, the standardizing process reduces the amplitude of any significant P300 complex diminishing its
403 automatic interpretation capability.

404 To further extend the capabilities of this method, it would be desirable to implement a multichannel
405 version. The straightforward extension of concatenating the obtained descriptors results in high dimensional
406 feature vector, while other variants that merge descriptors per channel may diminish the mutual information
407 between different channels. Hitherto variants using color versions of SIFT (Van De Sande et al., 2010),
408 where different color bands are mapped to electrode channels, have been explored without substantial
409 success.

410 In our opinion, the best benefit of the presented method is that a closer collaboration of the field of BCI
411 with physicians can be fostered (Chavarriaga et al., 2017), since this procedure intent to imitate human
412 visual observation. Automatic classification of patterns in EEG that are specifically identified by their
413 shapes like K-Complex, Vertex Waves, Positive Occipital Sharp Transient (Hartman, 2005) are a prospect
414 future work to be considered. We are currently working in unpublished material analyzing K-Complex
415 components that could eventually provide assistance to physicians to locate these EEG patterns, specially in
416 long recording periods, frequent in sleep research (Michel and Murray, 2012). Additionally, it can be used
417 for artifact removal which is performed on many occasions by visually inspecting signals. This is due to
418 the fact that the descriptors are a direct representation of the shape of signal waveforms. In line with these
419 applications, it can be used to build a database (Chavarriaga et al., 2017) of quantitative representations of
420 waveforms and improve atlases (Hartman, 2005), which are currently based on qualitative descriptions of
421 signal shapes.

CONFLICT OF INTEREST STATEMENT

422 The authors declare that the research was conducted in the absence of any commercial or financial
423 relationships that could be construed as a potential conflict of interest.

AUTHOR CONTRIBUTIONS

424 This work is part of the PhD thesis of RR which is directed by JS and codirected by AV.

FUNDING

425 This project was supported by the ITBACyT-15 funding program issued by ITBA University from Buenos
426 Aires, Argentina.

REFERENCES

- 427 Alvarado-González, M., Garduño, E., Bribiesca, E., Yáñez-Suárez, O., and Medina-Bañuelos, V. (2016).
428 P300 Detection Based on EEG Shape Features. *Computational and Mathematical Methods in Medicine*,
429 1–14doi:10.1155/2016/2029791
- 430 Arandjelovic, R. and Zisserman, A. (2012). Three things everyone should know to improve object retrieval.
431 In *2012 IEEE Conference on Computer Vision and Pattern Recognition(CVPR)* (Providence, RI, USA),
432 2911–2918. doi:10.1109/CVPR.2012.6248018
- 433 Berger, S., Schneider, G., Kochs, E., and Jordan, D. (2017). Permutation Entropy: Too Complex a Measure
434 for EEG Time Series? *Entropy 2017, Vol. 19, Page 692* 19, 692. doi:10.3390/E19120692
- 435 Boiman, O., Shechtman, E., and Irani, M. (2008). In defense of nearest-neighbor based image classification.
436 *26th IEEE Conference on Computer Vision and Pattern Recognition, CVPR* doi:10.1109/CVPR.2008.
437 4587598
- 438 Bresenham, J. E. (1965). Algorithm for computer control of a digital plotter. *IBM Systems Journal* 4,
439 25–30
- 440 Brunner, C., Blankertz, B., Cincotti, F., Kübler, A., Mattia, D., Miralles, F., et al. (2014). BNCI Horizon
441 2020 – Towards a Roadmap for Brain / Neural Computer Interaction. *Lecture Notes in Computer Science*
442 8513, 475–486
- 443 Carlson, T. and del R. Millan, J. (2013). Brain-controlled wheelchairs: A robotic architecture. *IEEE*
444 *Robotics & Automation Magazine* 20, 65–73. doi:10.1109/MRA.2012.2229936
- 445 Casarotto, S., Bianchi, A., Cerutti, S., and Chiarenza, G. (2005). Dynamic time warping in the analysis of
446 event-related potentials. *IEEE Engineering in Medicine and Biology Magazine* 24, 68–77. doi:10.1109/
447 MEMB.2005.1384103
- 448 Chavarriaga, R., Fried-Oken, M., Kleih, S., Lotte, F., and Scherer, R. (2017). Heading for new shores!
449 Overcoming pitfalls in BCI design. *Brain-Computer Interfaces* 4, 60–73. doi:10.1080/2326263X.2016.
450 1263916
- 451 Clerc, M., Bougrain, L., and Lotte, F. (2016). *Brain-computer interfaces, Technology and applications*
452 2(Cognitive Science) (London, United Kingdom: ISTE Ltd. and Wiley)
- 453 De Vos, M. and Debener, S. (2014). Mobile EEG: Towards brain activity monitoring during natural action
454 and cognition. *International Journal of Psychophysiology* 91, 1–2. doi:10.1016/j.ijpsycho.2013.10.008
- 455 Farwell, L. A. and Donchin, E. (1988). Talking off the top of your head: toward a mental prosthesis utilizing
456 event-related brain potentials. *Electroencephalography and clinical neurophysiology* 70, 510–23
- 457 Guger, C., Allison, B., and Lebedev, M. (2017). Introduction. In *Brain Computer Interface Research: A*
458 *State of the Art Summary* 6 (Springer, Cham). 1–8. doi:10.1007/978-3-319-64373-1_1
- 459 Guger, C., Daban, S., Sellers, E., Holzner, C., Krausz, G., Carabalona, R., et al. (2009). How many people
460 are able to control a P300-based brain-computer interface (BCI)? *Neuroscience Letters* 462, 94–98.
461 doi:10.1016/j.neulet.2009.06.045
- 462 Hartman, a. L. (2005). *Atlas of EEG Patterns*, vol. 65 (Philadelphia, PA, USA: Lippincott Williams &
463 Wilkins). doi:10.1212/01.wnl.0000174180.41994.39

- 464 Hu, L., Mouraux, A., Hu, Y., and Iannetti, G. D. (2010). A novel approach for enhancing the signal-to-noise
465 ratio and detecting automatically event-related potentials (ERPs) in single trials. *NeuroImage* 50, 99–111.
466 doi:10.1016/j.neuroimage.2009.12.010
- 467 Hubel, D. H. and Wiesel, T. N. (1962). Receptive fields, binocular interaction and functional architecture in
468 the cat's visual cortex. *The Journal of Physiology* 160, 106–154. doi:10.1113/jphysiol.1962.sp006837
- 469 Huggins, J. E., Alcaide-Aguirre, R. E., and Hill, K. (2016). Effects of text generation on P300 brain-
470 computer interface performance. *Brain-Computer Interfaces* 3, 112–120. doi:10.1080/2326263X.2016.
471 1203629
- 472 Jure, F., Carrere, L., Gentiletti, G., and Tabernig, C. (2016). BCI-FES system for neuro-rehabilitation of
473 stroke patients. *Journal of Physics: Conference Series* 705, 1–8. doi:10.1088/1742-6596/705/1/012058
- 474 Knuth, K. H., Shah, A. S., Truccolo, W. A., Ding, M., Bressler, S. L., and Schroeder, C. E. (2006).
475 Differentially variable component analysis: Identifying multiple evoked components using trial-to-trial
476 variability. *Journal of Neurophysiology* 95, 3257–3276. doi:10.1152/jn.00663.2005
- 477 Krusienski, D. J., Sellers, E. W., Cabestaing, F., Bayoudh, S., McFarland, D. J., Vaughan, T. M., et al.
478 (2006). A comparison of classification techniques for the P300 Speller. *Journal of Neural Engineering*
479 3, 299–305. doi:10.1088/1741-2560/3/4/007
- 480 Liang, N. and Bougrain, L. (2008). Averaging techniques for single-trial analysis of oddball event-related
481 potentials. *4th International Brain-Computer Interface Workshop*, 1–6
- 482 Lotte, F., Bougrain, L., Cichocki, A., Clerc, M., Congedo, M., Rakotomamonjy, A., et al. (2018). A review
483 of classification algorithms for EEG-based brain–computer interfaces: a 10 year update. *Journal of
484 Neural Engineering* 15, 031005. doi:10.1088/1741-2552/aab2f2
- 485 Lotte, F., Faller, J., Guger, C., Renard, Y., Pfurtscheller, G., Lécuyer, A., et al. (2013). *Combining BCI
486 with Virtual Reality: Towards New Applications and Improved BCI* (Berlin, Heidelberg: Springer Berlin
487 Heidelberg). 197–220. doi:10.1007/978-3-642-29746-5_10
- 488 Lowe, G. (2004). SIFT - The Scale Invariant Feature Transform. *International Journal* 2, 91–110
- 489 Madarame, T., Tanaka, H., Inoue, T., Kamata, M., and Shino, M. (2008). The development of a brain
490 computer interface device for amyotrophic lateral sclerosis patients. In *Conference Proceedings -
491 IEEE International Conference on Systems, Man and Cybernetics* (Singapore: IEEE), 2401–2406.
492 doi:10.1109/ICSMC.2008.4811654
- 493 Mak, J. N., McFarland, D. J., Vaughan, T. M., McCane, L. M., Tsui, P. Z., Zeitlin, D. J., et al. (2012). EEG
494 correlates of P300-based brain-computer interface (BCI) performance in people with amyotrophic lateral
495 sclerosis. *Journal of Neural Engineering* 9. doi:10.1088/1741-2560/9/2/026014
- 496 McCane, L. M., Heckman, S. M., McFarland, D. J., Townsend, G., Mak, J. N., Sellers, E. W., et al.
497 (2015). P300-based brain-computer interface (BCI) event-related potentials (ERPs): People with
498 amyotrophic lateral sclerosis (ALS) vs. age-matched controls. *Clinical Neurophysiology* 126, 2124–2131.
499 doi:10.1016/j.clinph.2015.01.013
- 500 Michel, C. M. and Murray, M. M. (2012). Towards the utilization of EEG as a brain imaging tool.
501 *NeuroImage* 61, 371–385. doi:10.1016/j.neuroimage.2011.12.039
- 502 Mortensen, E. N., , and Shapiro, L. (2005). A sift descriptor with global context. In *2005 IEEE Computer
503 Society Conference on Computer Vision and Pattern Recognition (CVPR'05)* (San Diego, CA, USA),
504 vol. 1, 184–190. doi:10.1109/CVPR.2005.45
- 505 Nam, C. S., Li, Y., and Johnson, S. (2010). Evaluation of P300-based brain-computer interface in real-
506 world contexts. *International Journal of Human-Computer Interaction* 26, 621–637. doi:10.1080/
507 10447311003781326

- 508 Nijboer, F. and Broermann, U. (2009). Brain Computer Interfaces for Communication and Control in
509 Locked-in Patients. In *Graimann B., Pfurtscheller G., Allison B. (eds) Brain-Computer Interfaces. The*
510 *Frontiers Collection*. (Springer Berlin Heidelberg). 185–201. doi:10.1007/978-3-642-02091-9_11
- 511 Novak, D., Sigrist, R., Gerig, N. J., Wyss, D., Bauer, R., Gotz, U., et al. (2018). Benchmarking brain-
512 computer interfaces outside the laboratory: The cybathlon 2016. *Frontiers in Neuroscience* 11, 756.
513 doi:10.3389/fnins.2017.00756
- 514 Polich, J. (2007). Updating P300: An integrative theory of P3a and P3b. *Clinical Neurophysiology* 118,
515 2128–2148. doi:10.1016/j.clinph.2007.04.019
- 516 Rakotomamonjy, A. and Guigue, V. (2008). BCI Competition III: Dataset II- Ensemble of SVMs for BCI
517 P300 Speller. *IEEE Transactions on Biomedical Engineering* 55, 1147–1154. doi:10.1109/TBME.2008.
518 915728
- 519 Ramele, R., Villar, A. J., and Santos, J. M. (2016). BCI classification based on signal plots and SIFT
520 descriptors. In *4th International Winter Conference on Brain-Computer Interface, BCI 2016* (Yongpyong:
521 IEEE), 1–4. doi:10.1109/IWW-BCI.2016.7457454
- 522 [Dataset] Ramele, R., Villar, A. J., and Santos, J. M. (2017). P300-dataset rrid scr_015977.
523 <https://www.kaggle.com/rramele/p300samplingdataset>
- 524 Rao, R. P. N. (2013). *Brain-Computer Interfacing: An Introduction* (New York, NY, USA: Cambridge
525 University Press)
- 526 Renard, Y., Lotte, F., Gibert, G., Congedo, M., Maby, E., Delannoy, V., et al. (2010). OpenViBE: An
527 Open-Source Software Platform to Design, Test, and Use Brain–Computer Interfaces in Real and Virtual
528 Environments. *Presence: Teleoperators and Virtual Environments* 19, 35–53. doi:10.1162/pres.19.1.35
- 529 Rey-Otero, I. and Delbracio, M. (2014). Anatomy of the SIFT Method. *Image Processing On Line* 4,
530 370–396. doi:<http://dx.doi.org/10.5201/ipol.2014.82>
- 531 Riccio, A., Simione, L., Schettini, F., Pizzimenti, A., Inghilleri, M., Belardinelli, M. O., et al. (2013).
532 Attention and P300-based BCI performance in people with amyotrophic lateral sclerosis. *Frontiers in
533 Human Neuroscience* 7, 732. doi:10.3389/fnhum.2013.00732
- 534 Riener, R. and Seward, L. J. (2014). Cybathlon 2016. *2014 IEEE International Conference on Systems,
535 Man, and Cybernetics (SMC)*, 2792–2794doi:10.1109/SMC.2014.6974351
- 536 Schalk, G., McFarland, D. J., Hinterberger, T., Birbaumer, N., and Wolpaw, J. R. (2004). BCI2000: a
537 general-purpose brain-computer interface (BCI) system. *IEEE transactions on bio-medical engineering*
538 51, 1034–43. doi:10.1109/TBME.2004.827072
- 539 Scholkopf, B. and Smola, A. J. (2001). *Learning with kernels: support vector machines, regularization,
540 optimization, and beyond* (Cambridge, MA, USA: MIT Press)
- 541 Schomer, D. L. and Silva, F. L. D. (2010). *Niedermeyer's Electroencephalography: Basic Principles,
542 Clinical Applications, and Related Fields* (Philadelphia, PA, USA: Walters Klutter -Lippincott Williams
543 & Wilkins)
- 544 Sellers, E. W., Kübler, A., and Donchin, E. (2006). Brain-computer interface research at the University of
545 South Florida cognitive psychophysiology laboratory: The P300 speller. *IEEE Transactions on Neural
546 Systems and Rehabilitation Engineering* 14, 221–224. doi:10.1109/TNSRE.2006.875580
- 547 Tibon, R. and Levy, D. A. (2015). Striking a balance: analyzing unbalanced event-related potential data.
548 *Frontiers in psychology* 6, 555. doi:10.3389/fpsyg.2015.00555
- 549 Van De Sande, K., Gevers, T., and Snoek, C. (2010). Evaluating color descriptors for object and
550 scene recognition. *IEEE Transactions on Pattern Analysis and Machine Intelligence* 32, 1582–1596.
551 doi:10.1109/TPAMI.2009.154

- 552 Van Drongelen, W. (2006). *Signal processing for neuroscientists: an introduction to the analysis of*
553 *physiological signals* (London, United Kingdom: Academic press)
- 554 Vedaldi, A. and Fulkerson, B. (2010). VLFeat - An open and portable library of computer vision algorithms.
555 *Design 3*, 1–4. doi:10.1145/1873951.1874249
- 556 Wolpaw, J. and E., W. (2012). *Brain-Computer Interfaces: Principles and Practice* (New York, NW, USA:
557 Oxford University Press)
- 558 Yamaguchi, T., Fujio, M., Inoue, K., and Pfurtscheller, G. (2009). Design method of morphological
559 structural function for pattern recognition of EEG signals during motor imagery and cognition. In *Fourth*
560 *International Conference on Innovative Computing, Information and Control (ICICIC)* (Kaohsiung,
561 Republic of China), 1558–1561. doi:10.1109/ICICIC.2009.161

5 APPENDIX

562 This section describes the differences between the HIST algorithm proposed in this work and the SIFT
563 Descriptor (Vedaldi and Fulkerson, 2010).

564 The two most important modifications are:

- 565 • SIFT Detector and custom frame: The SIFT Detector provides the keypoint localization information in
566 the standard SIFT method. The keypoint localization information is stored in a *frame* data structure
567 which is composed of the keypoint center location (x_{kp}, y_{kp}), patch scale s and patch orientation ϕ :
568 (x_{kp}, y_{kp}, s, ϕ). In the HIST proposal the keypoint location and patch parameters are directly specified
569 over the plot image in order to detect the signal waveform (see Section 2.2.3) and the SIFT Detector is
570 not used.
- 571 • Patch scale: Whereas in the standard SIFT implementation the patch is a squared region and there is
572 only one SIFT scale parameter, in HIST a different scale parameter can be assigned to the horizontal
573 and vertical axis. This is a very important modification because otherwise signal plots which extend
574 only on the horizontal direction of the plot image could not be entirely covered. By using a rectangular
575 patch, there isn't any constraint on its size and it can be adjusted by neurophysiological priors to map
576 any expected waveform based on Equations 10 and 11.

577 Additionally, other changes are implemented where specific steps of the SIFT Descriptor were not found
578 to be useful to characterize signal waveforms:

- 579 • Patch orientation: We verified experimentally that the patch orientation ϕ does not provide any extra
580 utility for the extraction of characteristic waveforms from plots. Hence, this patch orientation is fixed
581 to zero (vertical, pointing upwards in Figure 4).
- 582 • Rotations: SIFT was designed to allow affine invariance, i.e. to be robust to rotations and scale
583 modifications of patterns in images. It was not found, so far, of any utility to rotate the patch to capture
584 the signal waveform.
- 585 • Octave selection: A gradient image is used to obtain the oriented gradients and calculate the histogram
586 of gradient orientations. In SIFT, these gradient images are downsampled and smoothed by a Gaussian
587 filter. The SIFT Descriptor calls *octave* to each downsampling level (Lowe, 2004; Rey-Otero and
588 Delbracio, 2014). The standard SIFT Descriptor estimates the octave to use on the gradient image
589 based on the image size and patch parameters. The HIST method uses only the zero octave which
590 means that the gradient image has the same size as the original image, without any downsampling
591 operation.

- 592 • Gradient image smoothing: Additionally, the SIFT Descriptor performs an initial smoothing operation
593 by applying a Gaussian filter on the gradient image regardless of the octave. In the HIST method, this
594 operation is not implemented.
- 595 • Descriptor Gaussian weighting: On the standard SIFT Descriptor, a Gaussian weighting operation
596 is performed on the calculated SIFT descriptor to increase the importance of gradients from pixels
597 closer to the center of the patch. For the HIST method, this is found to be in detriment of the waveform
598 characterization and is not used.
- 599 • SIFT descriptor codification: The SIFT descriptor d is a 128-dimension feature vector, as described in
600 Section 2.1.3. Histogram values are floating point numbers, all positive, and they are accumulated on
601 each coordinate of this vector. Once all the gradients are summarized, the following operations are
602 performed:
- 603 • The descriptor is ℓ -2 normalized (i.e all the values are divided by the euclidean norm of the
604 descriptor).
- 605 • Each value is clamped to 0.2. This means that any value above 0.2 is set to 0.2.
- 606 • The descriptor is ℓ -2 re-normalized again (Rey-Otero and Delbracio, 2014).

607 This generates a 128-vector of floating point numbers, between $[0, 1]$. In the HIST implementation,
608 these values are rescaled to $[-1, 1]$ in order to use the cosine distance (Arandjelovic and Zisserman,
609 2012) on Equations 9 and 8. Finally, output values are cast to floating point numbers (i.e. floats).
610 yielding an effective 128-vector of floats between $[-1, 1]$.

Table 1. Character recognition rates for the public dataset of ALS patients using the Histogram of Gradient (HIST) calculated from single-channel plots. Performance rates using single-channel signals with the SVM classifier are shown for comparison. The best performing channel *bpc* for each method is visualized

Participant	<i>bpc</i>	HIST	<i>bpc</i>	Single Channel SVM
1	Cz	35%	Cz	15%
2	Fz	85%	PO8	25%
3	Cz	25%	Fz	5%
4	PO8	55%	Oz	5%
5	PO7	40%	P3	25%
6	PO7	60%	PO8	20%
7	PO8	80%	Fz	30%
8	PO7	95%	PO7	85%

Table 2. Character recognition rates for the own dataset of healthy subjects using the Histogram of Gradient (HIST) calculated from single-channel plots. Performance rates using single-channel signals with the SVM classifier are shown for comparison. The best performing channel *bpc* for each method is visualized.

Participant	<i>bpc</i>	HIST	<i>bpc</i>	Single Channel SVM
1	Oz	40%	Cz	10%
2	PO7	30%	Cz	5%
3	P4	40%	P3	10%
4	P4	45%	P4	35%
5	P4	60%	P3	10%
6	Pz	50%	P4	25%
7	PO7	70%	P3	30%
8	P4	50%	PO7	10%

Table 3. Character recognition rates and the best performing channel *bpc* for the public dataset of ALS patients using the Histogram of Gradient (HIST) (repeated here for comparison purposes). Performance rates obtained by SWLDA and SVM classification algorithms with a multichannel concatenated feature.

Participant	<i>bpc</i> for HIST	HIST	Multichannel SWLDA	Multichannel SVM
1	Cz	35%	45%	40%
2	Fz	85%	30%	50%
3	Cz	25%	65%	55%
4	PO8	55%	40%	50%
5	PO7	40%	35%	45%
6	PO7	60%	35%	70%
7	PO8	80%	60%	35%
8	PO7	95%	90%	95%

Table 4. Character recognition rates and the best performing channel *bpc* for the own dataset of healthy subjects using the Histogram of Gradient (HIST) (repeated here for comparison purposes). Performance rates obtained by SWLDA and SVM classification algorithms with a multichannel concatenated feature.

Participant	<i>bpc</i> for HIST	HIST	Multichannel SWLDA	Multichannel SVM
1	Oz	40%	65%	40%
2	PO7	30%	15%	10%
3	P4	40%	50%	25%
4	P4	45%	40%	20%
5	P4	60%	30%	20%
6	Pz	50%	35%	30%
7	PO7	70%	25%	30%
8	P4	50%	35%	20%

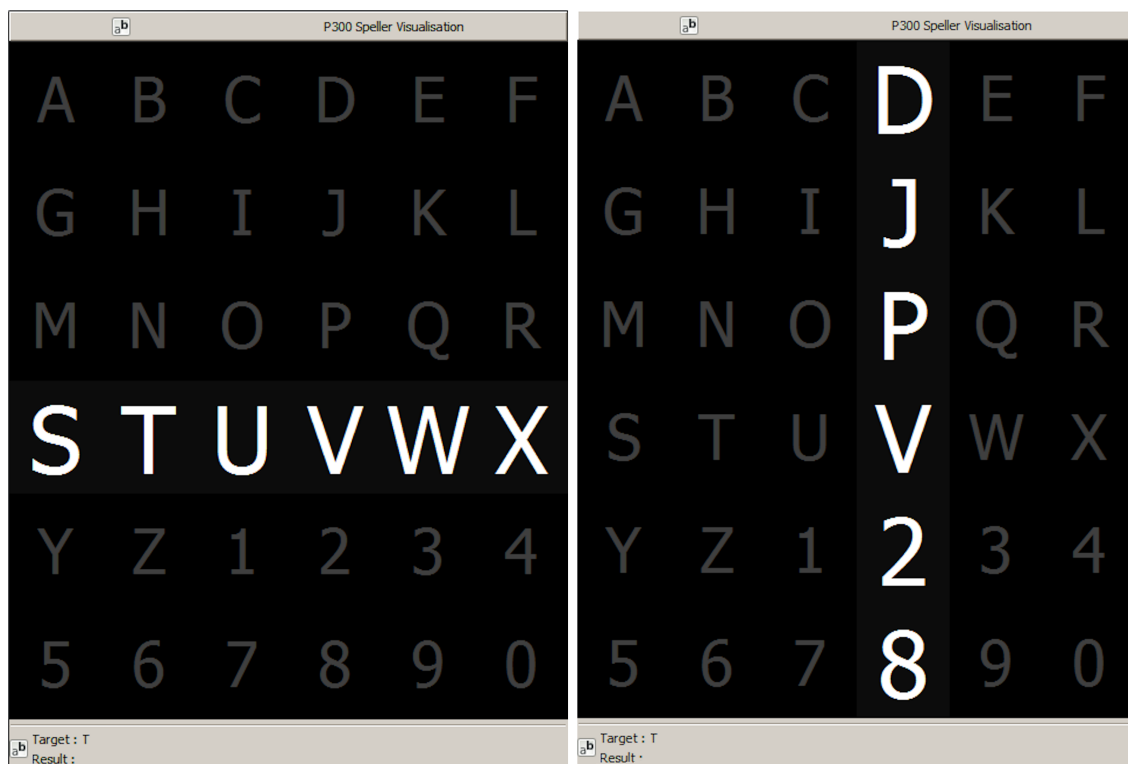


Figure 1. Example of the 6×6 Speller Matrix used in the study obtained from the OpenVibe software. Rows and columns flash in random permutations.

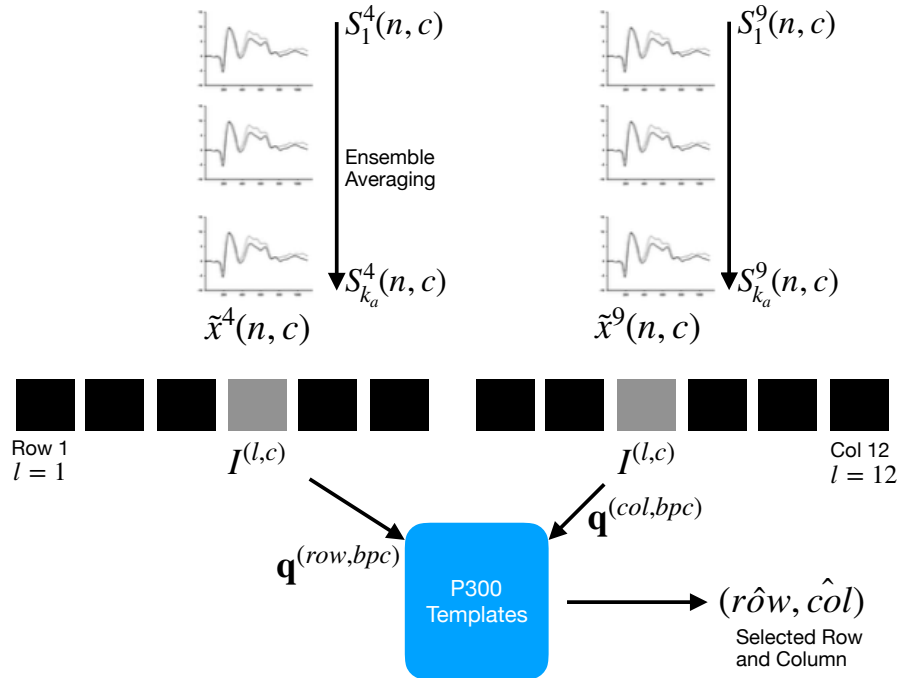


Figure 2. For each column and row, an averaged, standardized and scaled signal $\tilde{x}^l(n, c)$ is obtained from the segments S_i^l corresponding to the k_a intensification sequences with $1 \leq i \leq k_a$ and location l varying between 1 and 12. From the averaged signal, the image $I^{(l,c)}$ of the signal plot is generated and each descriptor is computed. By comparing each descriptor against the set of templates, the P300 ERP can be detected, and finally the desired letter from the matrix can be inferred.

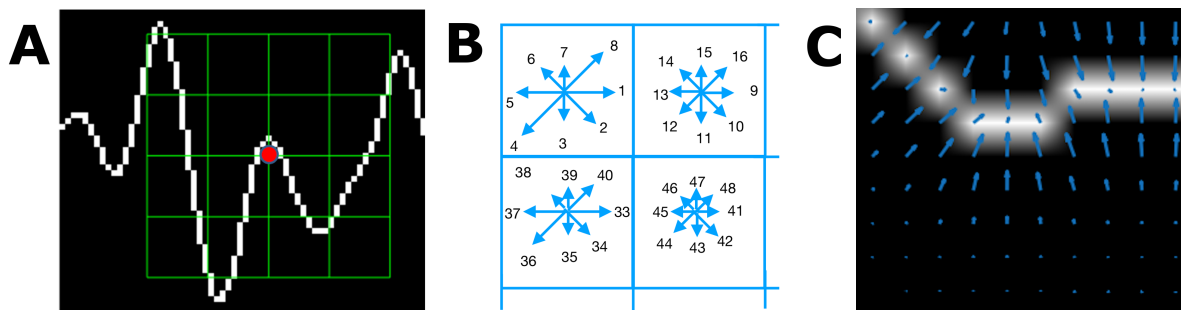


Figure 3. (A) Example of a plot of the signal, a keypoint and the corresponding patch. (B) A scheme of the orientation's histogram computation. Only the upper-left four blocks are visible. The first eight orientations of the first block, are labeled from 1 to 8 clockwise. The orientation of the second block $B_{1,2}$ is labeled from 9 to 16. This labeling continues left-to-right, up-down until the eight orientations for all the sixteen blocks are assigned. They form the corresponding descriptor of 128 coordinates. The length of each arrow represents the value of the histogram on each direction for each block. (C) Vector field of oriented gradients. Each pixel is assigned an orientation and magnitude calculated using finite differences.

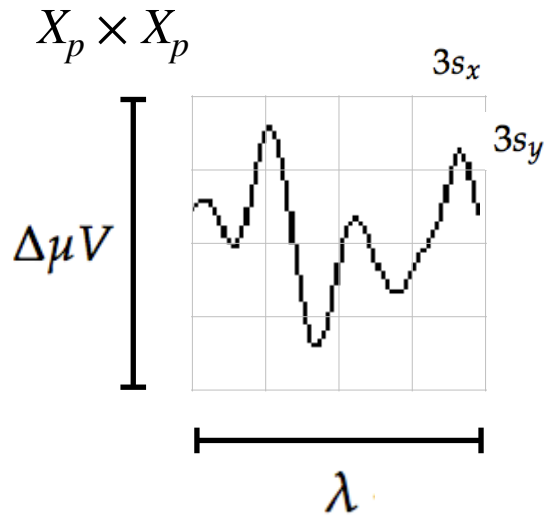


Figure 4. The scale of local patch is selected in order to capture the whole transient event. The size of the patch is $X_p \times X_p$ pixels. The vertical size consists of 4 blocks of size $3s_y$ pixels which is high enough as to contain the signal $\Delta\mu V$, the peak-to-peak amplitude of the transient event. The horizontal size includes 4 blocks of $3s_x$ and covers the entire duration in seconds of the transient signal event, λ .

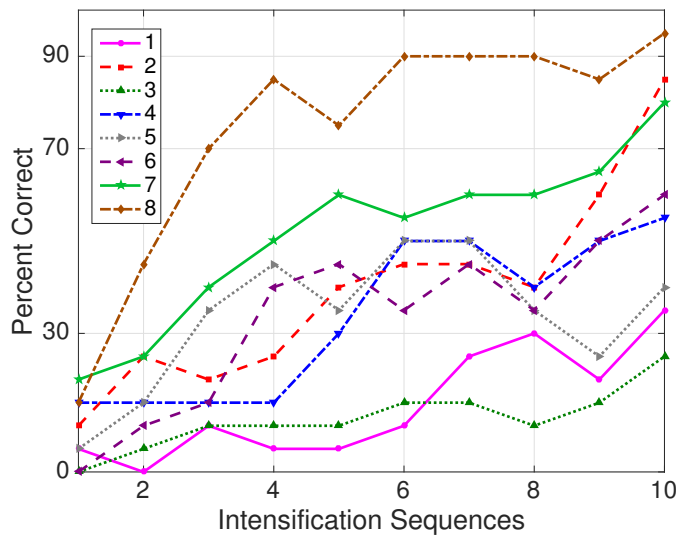


Figure 5. Performance curves for the eight subjects included in the dataset of ALS patients. Three out of eight subjects achieved the necessary performance to implement a valid P300 speller.

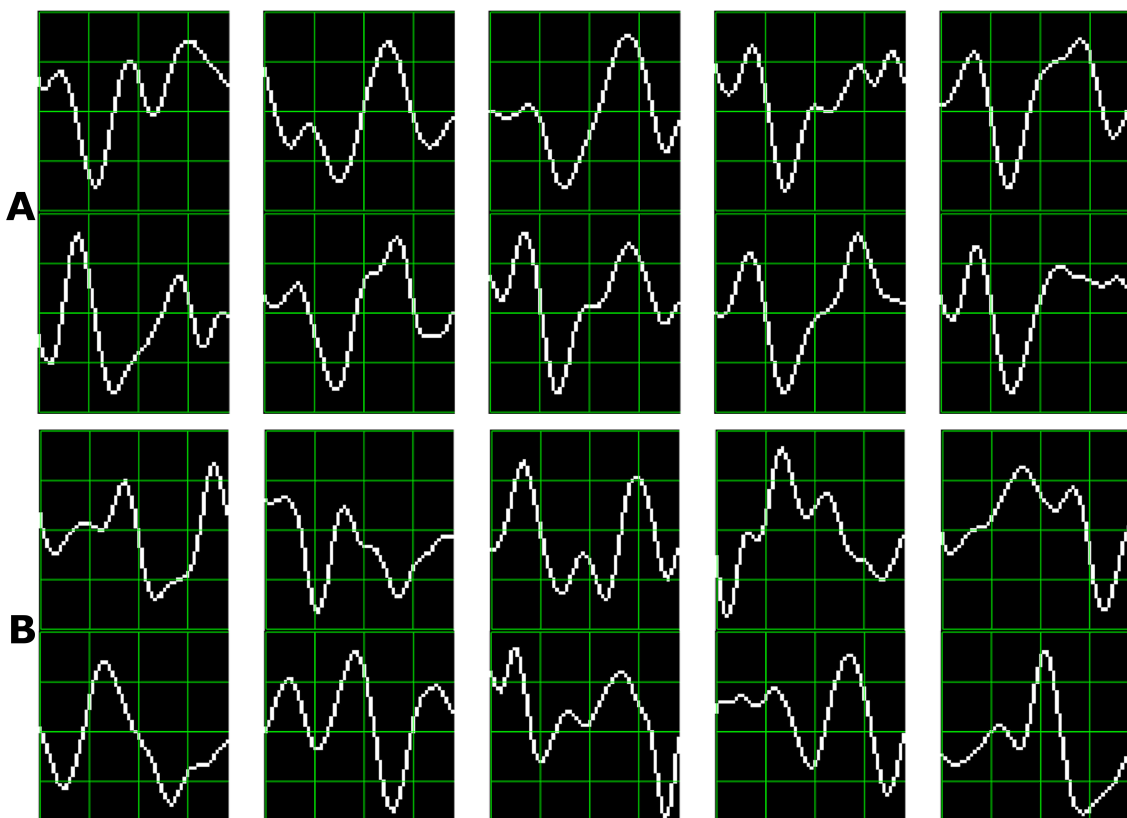


Figure 6. Ten sample P300 template patches for subjects 8 (A) and 3 (B) of the ALS Dataset. Downward deflection is positive polarity.